Journal of the Meteorological Society of Japan, Vol. 89, No. 5, pp. 455–474, 2011
DOI:10.2151/jmsj.2011-504

Leading Modes of East Asian Winter Climate Variability and Their Predictability: An Assessment of the APCC Multi-Model Ensemble

Soo-Jin SOHN

APEC Climate Center (APCC), Busan, South Korea

Chi-Yung TAM

Guy Carpenter Asia-Pacific Climate Impact Centre, City University of Hong Kong, Hong Kong, China

and

Chung-Kyu PARK

Korea Meteorological Administration (KMA), Seoul, South Korea

(Manuscript received 1 September 2009, in final form 2 June 2011)

Abstract

The variability and predictability of the East Asian (EA) winter climate has been studied, based on observed datasets and multi-model ensemble (MME) hindcast experiments archived at the APEC Climate Center (APCC). The focus is on the leading modes of wintertime variability over the eastern to northeastern part of Asia, which are identified based on multivariate EOF analysis of the monthly 850 hPa wind and temperature. The leading EA climate mode is characterized by continental-scale temperature anomalies covering a broad region from the northwestern flank of the Siberian high to northeast Asia. The second mode is associated with fluctuations of temperature and monsoon northerlies over the EA locations of Korea, Japan and eastern coastal China. Moreover, the first mode is found to be influenced by the Scandinavian (SCA) pattern, while the second mode is closely associated with the Eurasia (EU) pattern.

In general, the dominant circulation patterns of the EA wintertime variability from each MME member model compare well with their observational counterparts. However, the temporal variations of these modes are difficult to reproduce in the model simulations. The variation of the leading mode is found to be better predicted by most models, which leads to better predictions of the winter climate over continental northeast Asia, compared to the second mode. The MME performance is further assessed in the context of circulation changes during ENSO. It is found that most models have difficulty in capturing both the timing and strength of the observed second EA climate mode variations. Analysis based on observations shows that there is Rossby wave activity from Eurasia in early boreal winter during ENSO years. The Eurasian wave train, however, is either too weak or absent in the model simulations. Overall, these results highlight the difficulties in forecasting EA winter climate in the current framework of seasonal climate prediction.

1. Introduction

The climate in the East Asian (EA) region is greatly influenced by the monsoon circulation. An active EA winter monsoon is characterized by a strong Siberian high and frequent cold surges, which strongly affect

Corresponding author: Soo-Jin Sohn, APEC Climate Center (APCC), 1463 U-dong, Haeundae-gu, Busan 612020, Republic of Korea.
E-mail: jeenie7@apcc21.net

the local weather in the region (Chan 2005). Much effort has been made to understand the variability of the EA winter climate by meteorologists (Lau and Li 1984; Zhang et al. 1997a; Gong et al. 2001; Wu and Wang 2002; Jhun and Lee 2004; Takaya and Nakamura 2005). Fluctuations from the synoptic to intraseasonal scale have been identified (Murakami 1979; Pan and Zhou 1985; Takaya and Nakamura 2005). The interannual to interdecadal variability of the EA circulation was also examined in some observational studies (see, e.g., Zhang et al. 1997a; Chen et al. 2000; Zhu et al. 2005).

There are a number of climate modes which contribute to the EA wintertime variability. On the interdecadal timescale, Jhun and Lee (2004) showed that the Arctic Oscillation (AO; Thompson and Wallace 2000) is closely related to the EA winter monsoon activity. Other studies suggest that the interannual variability of EA winter climate is associated with other climate modes besides AO. By analyzing the Siberian high activity and station temperature over eastern China, Gong et al. (2001) showed that both AO and the Eurasian pattern (EU pattern; Wallace and Gutzler 1981) affect the regional climate over East Asia in winter. Wu and Wang (2002) suggested that AO and the Siberian high can influence the EA monsoon through different mechanisms. In particular, AO is found to be related to climate variations north of 35°N in East Asia, while the impact of the Siberian high is felt along the East Asian coast. It should be mentioned that the Scandinavian (SCA) pattern (Barnston and Livezey 1987), a recurrent climate mode over Eurasia, also affects the wintertime circulation, over the northeastern part of Asia (Bueh and Nakamura 2007).

The El Nino and Southern Oscillation (ENSO), being the most important contributor of climate variability on the interannual timescale, also has an impact on the EA circulation. In particular, the EA winter monsoon flow over the coastal East Asia tends to be weaker during the mature phase of El Nino (Zhang et al. 1997a; Chen et al. 2000; Lau and Wang 2005). Wang et al. (2000) noted the existence of a Pacific-East Asia teleconnection pattern characterized by an anomalous anticyclone (cyclone) over the western Pacific during El Nino (La Nina) events. This affects the East Asian climate during the peak of ENSO. Wang et al. (2008) found that ENSO may have an impact on the winter climate over the mid to high latitude EA region, depending on the phase of the Pacific Decadal Oscillation (PDO).

Numerical models can be a powerful tool for studying the variability of the EA winter climate. They can generate internally consistent simulation datasets, which make up for the lack of high-quality data, and are useful for investigating physical mechanisms associated with the EA climate variability. Zhang et al. (1997b) evaluated simulations of the EA winter monsoon in the eight GCMs that participated in the Atmospheric Model Intercomparison Project (AMIP), focusing on synoptic features of the monsoon. However, there are still relatively few diagnostic studies on the GCM simulated EA wintertime circulation compared to that of the EA summer monsoon.

Hence, this study aims at diagnosing the climate models taking part in the APEC Climate Center (APCC) multi-model ensemble (MME) seasonal prediction, focusing on the leading modes of the winter climate variability over the eastern to northeastern part of Asia. The predictability of the EA circulation will also be addressed in the context of these climate modes. To the best of our knowledge, there is currently no EA winter climate predictability study based on MME hindcast experiments. The rest of this paper is organized as follows. Section 2 describes the model experiments and datasets being used; Section 3 presents the wintertime circulation characteristics and leading modes of the EA climate variability, and results based on observations and model simulations are compared. The predictability of the EA climate modes, together with the MME prediction during ENSO, is presented in Section 4. Summary and discussions can be found in Section 5.

2. Model experiments and datasets

Hindcast experiments examined in this study are based on seasonal prediction models participating in the APCC MME seasonal forecast. Hindcasts from five different models are considered: Seasonal Model Intercomparison Project/Historical Forecast Project (SMIP/HFP)-type experiments (Kang and Shukla 2006) based on the Global Climate Prediction System (GCPS) of the Seoul National University, Korea (Kang et al. 2004); the Global Data Assimilation and Prediction System (GDAPS) of Korea Meteorological Administration (Park et al. 2002); the Hydrometeorological Centre of Russia (HMC) model (Tolstykh 2003); the Japan Meteorological Agency (JMA) model (Kanamitsu et al. 1983), and Coupled Model Intercomparison Project (CMIP)-type experiments (Covey et al. 2003) from the National Centers for Environmental Prediction (NCEP) Coupled Forecast System (CFS) (Saha et al. 2006). All model simulations cover the common period of 1983/1984 to 2003/2004 for the December-to-February season. A brief summary of the model experiments is presented in Table 1.

For the SMIP-type or "retrospective forecast" exper-

Table 1. Description of the five climate models used in this study.

Acronym	Participating Institute (Member Economy)	Resolution	No. of ensemble members	Experimental Type (SST Specification)
GCPS	Seoul National University (Korea)	T63 L21	12	SMIP/ HFP* (Persisted / Predicted)
GDAPS	Korea Meteorological Administration (Korea)	T106 L21	20	SMIP / HFP (Persisted / Predicted)
HMC	Hydrometeorological Centre of Russia (Russia)	1.125°lat × 1.40625°lon L28	10	SMIP / HFP (Persisted)
JMA	Japan Meteorological Agency (Japan)	TL95 L40	5	SMIP / HFP (Persisted / Predicted)
NCEP CFS	National Centers for Environmental Prediction (USA)	T62L64 (Atmos.), 1/3°lat × 1°lon L40 (Ocean)	15	CMIP** (Predicted)

* Seasonal Model Intercomparison Project / Historical Forecast Project

** Couple Model Intercomparison Project

iments, models are initiated based on observed conditions one month prior to the target season. Persistent (Roads et al. 2001) or forecasted (Bengtsson et al. 1993) sea surface temperature (SST) anomalies are prescribed as the lower boundary condition in the hindcast experiments of GCPS, GDAPS, HMC, and JMA. GCPS and GDAPS use the global SST prediction from the Korea Meteorological Administration / Seoul National University (KMA/SNU) prediction system (Kug et al. 2007). JMA also uses the two-tiered method with SST based on a merge of persisted anomalies and prediction by the JMA CGCM for El-Nino prediction. NCEP CFS is a one-tier prediction system using a coupled ocean-atmosphere model. The atmospheric component of the CFS is the NCEP Global Forecast System (GFS) (Moorthi et al. 2001), and the oceanic component is the GFDL Modular Ocean Model version 3 (MOM 3) (Pacanowski and Griffies 1998).

National Centers for Environmental Prediction - National Center for Atmospheric Research (NCEP-NCAR) reanalysis products (Kalnay et al. 1996) covering the same common period are taken as the observational dataset in this study. Upper-air variables such as temperature, winds and geopotential height, as well as the sea-level pressure (SLP), are used. Data at the 850 hPa level under the ground are not considered in our analyses.

3. Dominant modes of EA winter climate variability

3.1 Wintertime circulation characteristics

For an overview of the wintertime circulation over the EA region, Fig. 1 gives the seasonal mean SLP, 850 hPa wind and temperature during the December-to-February

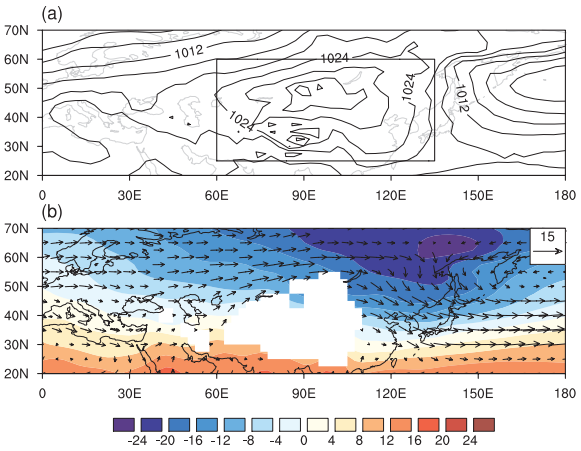

Fig. 1. (a) Climatological mean sea-level pressure (units: hPa), and (b) 850 hPa temperature (shading, see scale at bottom) and wind (arrows, see scale at upper right of panel; units: ms^{-1}) for the December-to-February period based on observations. The domain for EOF analysis is denoted by the rectangle surrounded by solid lines in (a).

period. The Asian winter monsoon is characterized by the presence of a continental-scale high pressure system centered in Siberia, covering most of the Eurasia region (see Fig. 1a). Due to this anticyclonic feature, prominent low-level winds have a dominant northerly component in East Asia (Fig. 1b). A strong, negative meridional temperature gradient exists over the coastal region in the midlatitude zone (see shading in Fig. 1b). Together with the wind field pattern, this implies intense

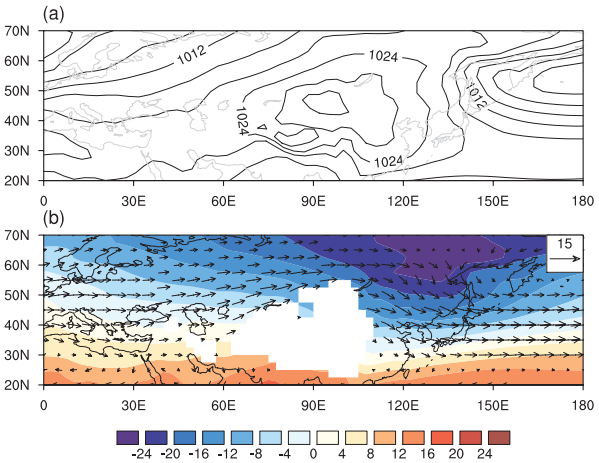

Fig. 2. Same Fig. 1 but for MME average.

cold temperature advection in East Asia during boreal winter.

The model simulated circulation statistics for the East Asia winter monsoon is presented. Figure 2 shows the MME mean of the DJF 850 hPa wind and temperature, calculated by taking the simple (un-weighted) average of the climatology from each model. Overall, there is broad agreement between model simulated circulation and observations. In particular, features such as the prominent low-level northerly wind in East Asia and the strong negative meridional temperature gradient over the eastern coastal region are well represented in the MME mean climatology. In other words, the models are capable of capturing the major features of the seasonal mean EA circulation. Compared to observations, the Siberian high given by the MME mean is displaced slightly to the south and the simulated SLP gradient is not as strong over northern Eurasia. We have also examined the climatologies from individual model runs. There are indeed some deviations in terms of the strength and exact locations of the maxima of the SLP field (figures not shown). Compared with SLP, agreement between individual models' and observed winds and temperature at the 850 hPa level is generally found to be better.

3.2 *Leading modes of EA winter climate variability*

In order to capture the dominant modes of the EA winter climate variability, multivariate empirical orthogonal function (EOF) analysis is employed using the temperature and meridional wind component at 850 hPa. The multivariate EOF analysis extends the conventional EOF by considering both spatial and inter-variable coherence. This often leads to more physical insight into the interactive processes within a complex system such as the ocean-atmosphere system (see Wang 1992 for more details). Also, because more than one climate mode are likely to affect the winter monsoon (see Introduction), an EOF approach is adopted here instead of using the more conventional choice of, say, a Siberian high index which characterizes the strength of the EA monsoon circulation. Observed monthly mean anomalies during the DJF period are used. To further compare the observed and model simulated EA winter climate variability, EOF analyses based on hindcast datasets are also carried out. For each individual model, monthly mean anomalies of the 850 hPa meridional wind and temperature from each ensemble run are used for the EOF computation. Based on the wintertime circulation characteristics just presented, the analysis domain of 60–135°E, 25–60°N is chosen (see rectangle in Fig. 1a). This region also encompasses the prominent high-pressure system over the Asian continent (see again Fig. 1). The first and second observed leading modes associated with temperature and wind variations account for about 36% and 19% of the domain integrated variance, respectively. To depict their related circulation patterns, regressions of meteorological variables onto their respective principal components (PC) are computed.

Figure 3 shows the regression maps of the 850 hPa temperature and winds onto the first PC, based on observations and model simulations. Only signals exceeding the 95% significance level are shown. (The statistical significance of the regression coefficients was evaluated using the two-tailed Student's t test; see, e.g., Zwiers and von Storch 1995.) The first EA winter climate mode from observations is characterized by continental-scale features, with cold anomalies covering a broad region from the northwestern flank of the Siberian high to the northeastern part of Asia. There is also a prominent warm temperature signal in the low levels over the high-latitude Arctic region. In the northern central part of the Asian continent, anomalous low-level northeasterlies can be found. This leads to strong cold air advection, accounting for the cold anomalies over the same locations. Regression coefficients of the SLP and geopotential height at 500 hPa onto the leading PC were also computed based on observations. The results (shown in Fig. 4a) indicate a positive SLP anomaly over the northern Eurasian continent to the Arctic, and negative ones in more southern latitudes (with most negative signals found in Southeast Asia and Europe). The height field regression (Fig. 4c) suggests an equivalent barotropic structure over the northwestern part of Eura-

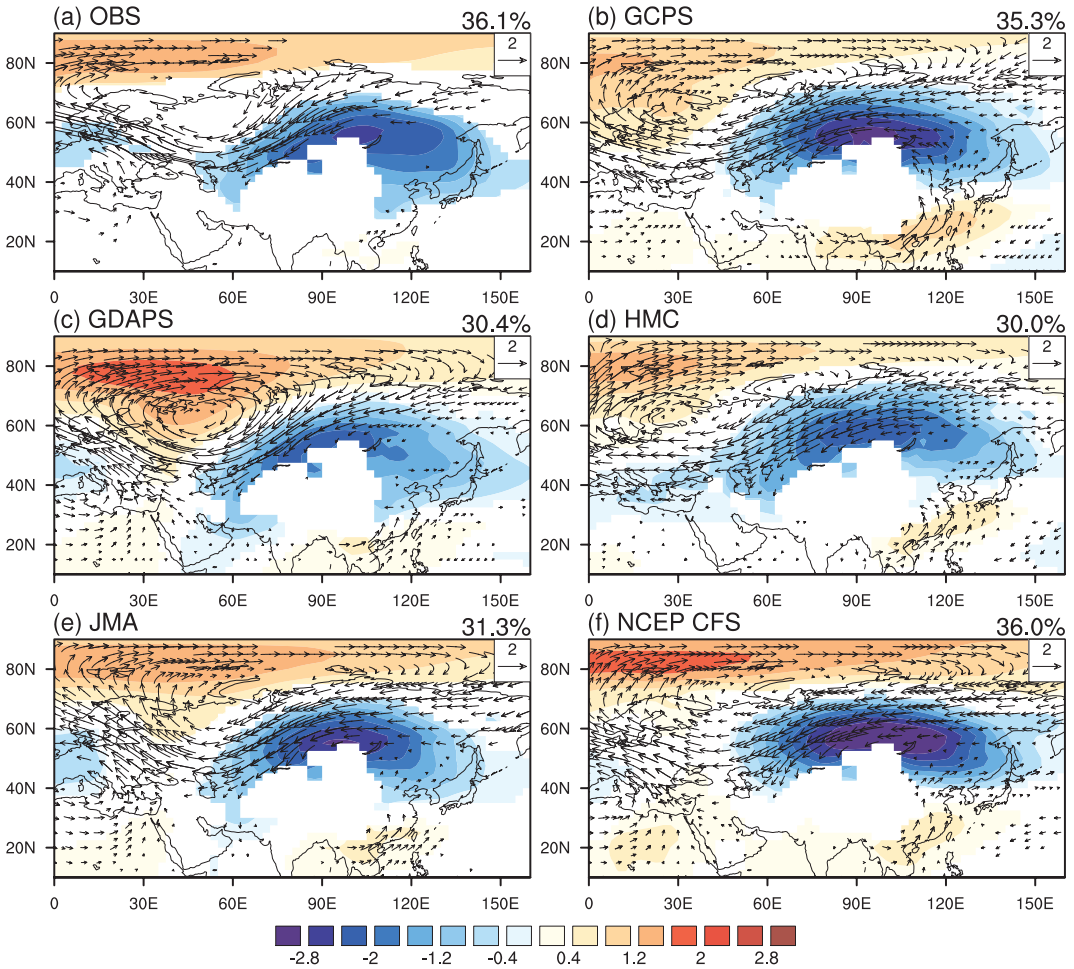

Fig. 3. Regression coefficients of the 850 hPa temperature (shading, see scale at bottom; units: °C) and winds (arrows, see scale at upper right of each panel; units: ms^{-1}) onto the first PC for the EA winter climate variability based on (a) observations and simulations from (b) GCPS, (c) GDAPS, (d) HMC, (e) JMA and (f) NCEP CFS. Shading and arrows denote, respectively, temperature and wind anomalies exceeding the 95% significance level based on the two-tailed Student's *t* test from observations and model simulations. The fractional variance explained by each mode for observations and GCM results are provided in upper right of each panel.

sia, while the circulation is more baroclinic over the continental northeast Asia. Overall, the distributions of the anomaly patterns of the 500-hPa geopotential height and SLP fields associated with the first mode are suggestive of the SCA pattern, with primary centers of action around the Scandinavian Peninsula, and the other two centers, with the opposite sign, located over the northeastern Atlantic and to the south of Lake Baikal (see Bueh and Nakamura 2007). As will be shown later, there is indeed a connection between this leading mode and the SCA pattern.

For the leading EA winter climate mode, results from individual models give significant warming over the Arctic region and cold anomalies over Eurasia and East Asia (see Figs. 3b–f). Prominent low-level northeasterly anomalies at about 60°N over central Asia are found in all model hindcast experiments. The model-simulated features of this mode are in good agreement with those from observations (see Fig. 3a). For most models, except GDAPS, the magnitude of cold anomalies associated with the first EA climate mode is also comparable to the observed. GDAPS gives temperature signals which are slightly weaker than those from other models over the continental northeast Asia.

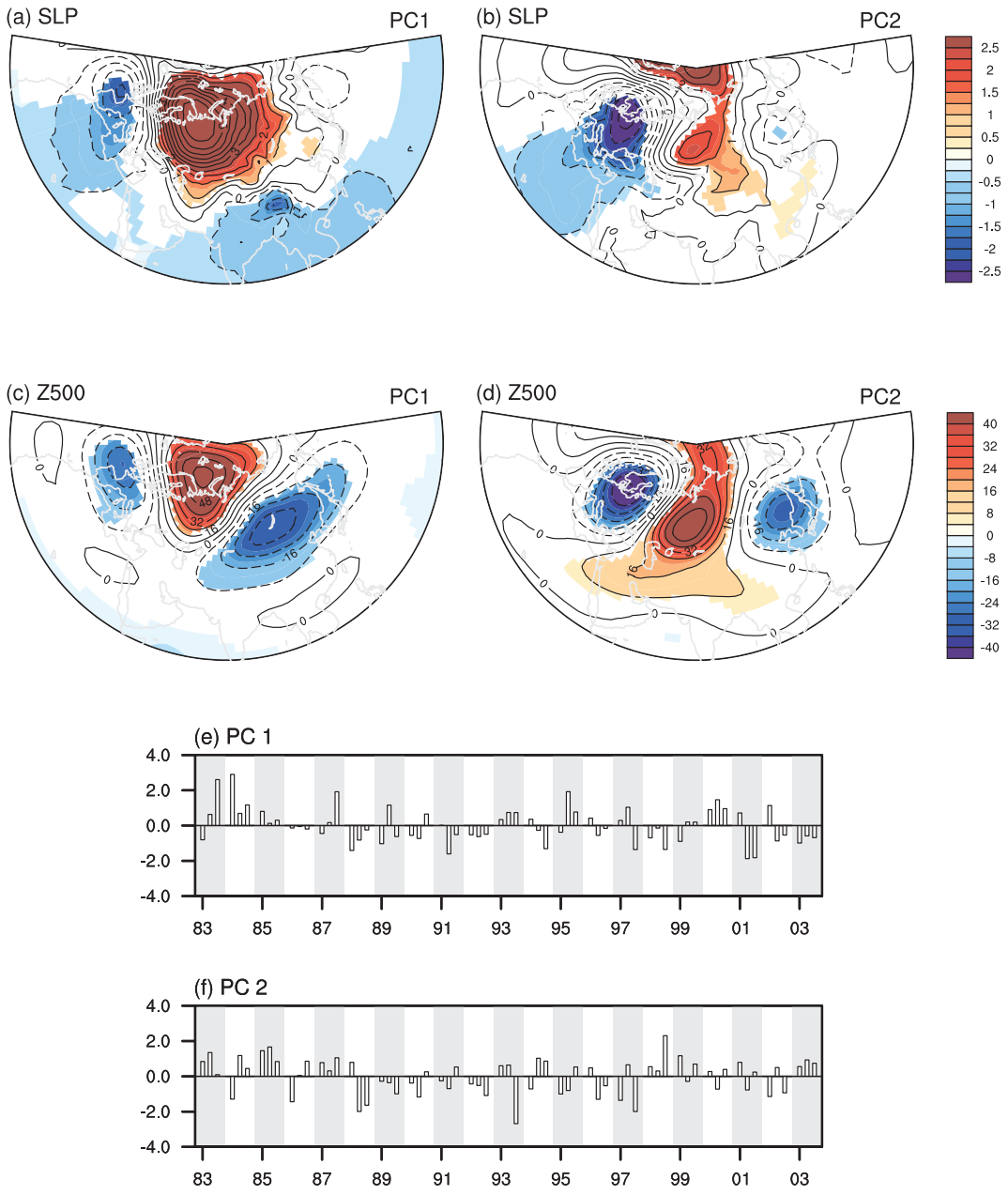

Fig. 4. Regression coefficients of (a, b) sea-level pressure (units: hPa) and (c, d) 500 hPa geopotential height (units: m) onto the first two PC for EA winter climate variability based on observations. Time series of the PCs for (e) the first EA winter climate mode and (f) the second mode. In (a), (b), (c), and (d), shading denotes values exceeding the 95% significance level.

Figure 5 shows the regression maps for the second EA climate mode based on observations and model simulations. For the observed second mode, circulation features are relatively more regional and also more wave-like compared with the first mode. A tri-pole pattern of temperature anomalies can be seen, with negative signals over Scandinavia and East Asia, and positive signals in between spanning the Caspian Sea and central Russia. Focusing on the EA region, prominent cooling exists over the eastern to southeastern coastal China,

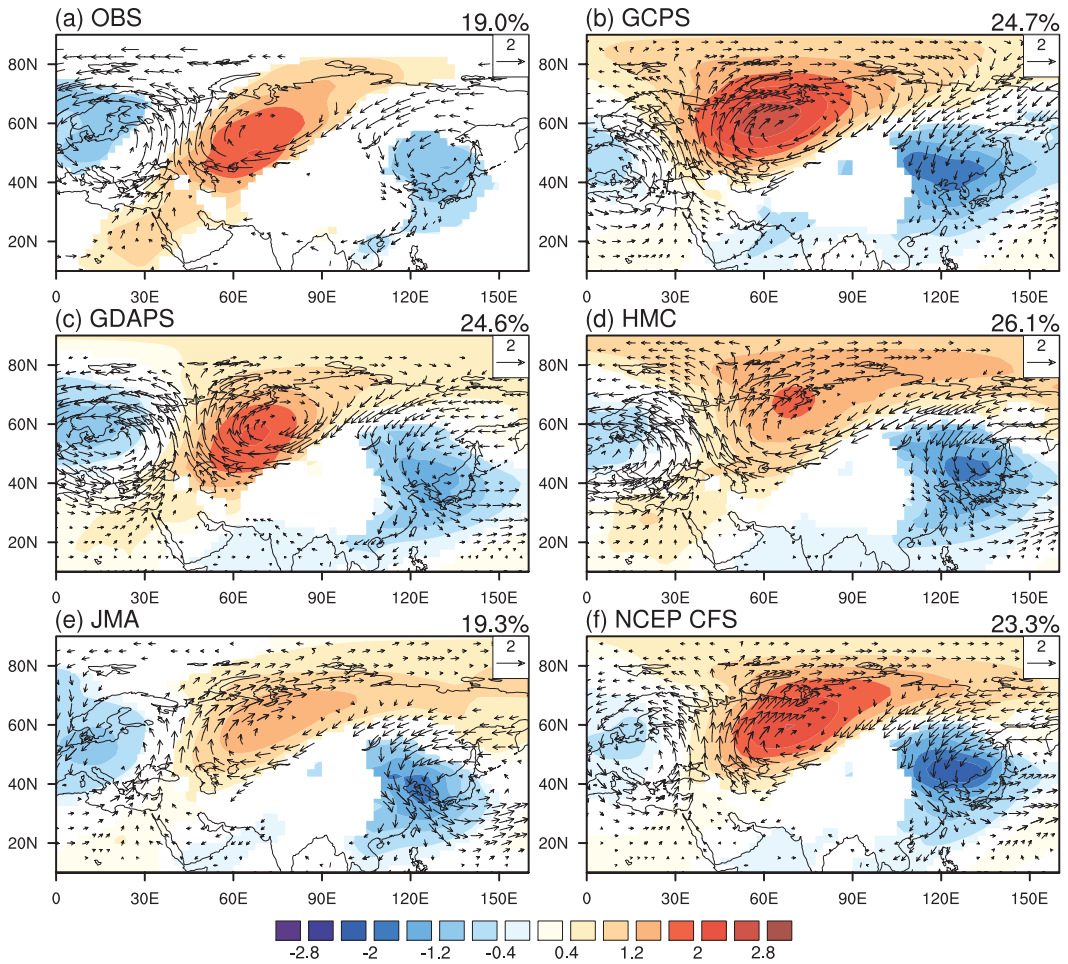

Fig. 5. Same as Fig. 3 but for the second PC.

Korean peninsula and Japan. The negative temperature anomaly can be attributed to the enhanced northerly wind in the same region. As mentioned before, this is where the mean temperature gradient is most negative. Stronger northerlies will therefore lead to intense cooling in these locations. Regression maps of SLP and the 500 hPa height field onto the second PC also show tripole patterns across the Eurasia continent (see Figs. 4b, d). In particular, there is a clear pattern of negative, positive and negative height field anomalies centered in northern Europe, central Eurasia and East Asia, respectively. It can be seen that these centers of action coincide well with those of the EU pattern (Wallace and Gutzler 1981). Compared with its observational counterpart (see Fig. 5a), it is obvious that the GCMs can simulate this second mode with a reasonable degree of realism. For instance, the tri-pole pattern of temperature anomalies across Eurasia can be seen in all hindcast runs. In the model environment, the anomalous anti-cyclonic (cyclonic) circulation is displaced slightly to the east of warm (cold) anomalies, suggesting a low-level baroclinic structure of this pattern. Over the mid-latitude to southern coastal East Asia, enhanced northerlies lead to strong cooling in the region.

The above results show that models can well capture the spatial structure of the leading modes of EA winter

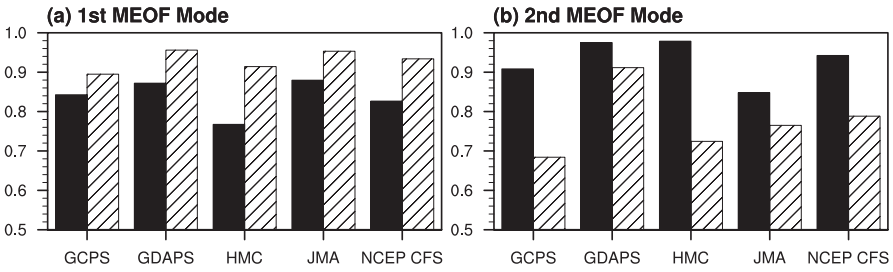

Fig. 6. Spatial pattern correlation coefficients between observations and model simulations for (a) the first mode and (b) second mode. Solid bars denote temperature and hatched bars denote the meridional wind component at 850 hPa.

Table 2. Correlation coefficients between the first and second PC time series and various climate indices for each month, as well as those computed using monthly values within the whole December-January-February period, from 1983/84 to 2003/04 based on observations. Values exceeding the 99% significance level are marked by double asterisks and those exceeding the 95% significance level are marked by single asterisks.

Indices	PC 1				PC 2			
	D	J	F	DJF Monthly	D	J	F	DJF Monthly
SCA	0.81*	0.52*	0.50*	0.68**	−0.59**	−0.28	−0.36	0.23
EU	−0.24	0.24	0.20	0.11	0.79**	0.96**	0.94**	0.90**
Nino3	0.10	−0.05	−0.34	−0.08	−0.49*	0.21	−0.25	−0.17
SH	0.48*	0.53*	0.62**	0.55**	0.06	0.47*	0.50**	0.35**
AO	−0.42	−0.52*	−0.40	−0.45**	−0.21	−0.62**	−0.32	−0.38**

climate variability. To quantify the ability of the models in reproducing the two leading EOF patterns, pattern correlation coefficients between the observed and simulated EOFs were computed. Results are shown in Fig. 6. For both EA climate modes, pattern correlations for the temperature as well as the meridional wind fields exceed the value of 0.6 for all hindcast datasets. It is clear that the model simulated EA winter climate modes resemble those from observations.

As mentioned in the Introduction, a number of studies show that the EA winter monsoon is influenced by a few major modes of climate variability. The above analysis also indicates that the leading EOFs of the EA winter climate variability partly resemble the SCA and EU patterns. To access the linkage between the EA climate and other climate modes in the observational record, the correlation coefficients between the first two PCs from the multivariate EOF analysis, and the SCA, EU, Nino3, Siberia high and AO indices are given in Table 2. The SCA pattern was identified by orthogonally rotated principal component analysis (RPCA) of Northern Hemisphere monthly mean 700-hPa geopotential height (Barnston and Livezey 1987). The monthly time series of the EU index is calculated based on the following formula (see Wallace and Gutzler 1981):

$$EU = -\frac{1}{4}Z^*(55^\circ\mathrm{N}, 20^\circ\mathrm{E}) + \frac{1}{2}Z^*(55^\circ\mathrm{N}, 75^\circ\mathrm{E}) - \frac{1}{4}Z^*(40^\circ\mathrm{N}, 145^\circ\mathrm{E}),$$

where Z^* denotes the normalized monthly mean height anomaly. The Siberian high index is defined as the SLP anomaly averaged over the area of 80–120°E, 40–60°N (see Jhun and Lee 2004). Finally, the AO index is defined as the first principal component of SLP to the north of 20°N (Thompson and Wallace 2000).

From the results based on the data for all months within the DJF season, it can be seen that the first mode is closely related to the SCA pattern for whole DJF period, as well as during each individual month. This suggests that, in the cold season, the positive phase of the pattern causes cold-air accumulation over a vast area extending from western Siberia to the regions around Lake Baikal and Lake Balkhash. The EU pattern is found to be strongly associated with the occurrence of the second EA climate mode, but unrelated to the first mode. The

strong positive correlation indicates that the EU pattern also plays an important role in regulating the EA winter monsoon (Gong et al. 2001). For each individual month within the boreal winter, a strong correlation between the second EA climate mode and the EU pattern is still present. The AO index is also correlated (negatively) with both of the leading PCs (significant at the 99% level). There is, however, stronger covariability between AO and the first mode, as compared to the second mode. This implies that a positive AO is likely to be associated with warmer than normal conditions in the central to northeastern part of continental Eurasia, consistent with results from a number of studies (Gong et al. 2001; Wu and Wang 2002). Also, both leading EA winter climate modes are related to the strength of the Siberian high, as evidenced by the high correlation between the SH index and the two leading PCs (with the exception of the December values of the second PC). Finally, the correlation between the two PCs and the Nino3 index is relatively low, except in December, during which the second mode seems to be associated with the occurrence of ENSO. A more detailed analysis on the relationship between ENSO and the EA winter climate modes will be given in Section 4.

We have also assessed the extent to which the two observed leading PCs can account for the temperature variations over East Asia. Over the region of 75–135°E, 40–60°N, the correlation coefficient between the leading PC time series and the area-averaged 850-hPa temperature from observations is −0.98. For the more southern domain of 110–150°E, 25–45°N, the correlation between the averaged temperature and the second PC is −0.46. The strong correlation suggests that these two leading modes are strong contributors to the EA wintertime variability. Finally, it is of interests to compare our EA winter climate modes, which focus on the mid-to-high latitude EA region, with other measures of the EA winter monsoon variability. In particular, we have computed the correlation between the EA winter monsoon index of Chen et al. (2000), which is defined as the sum of the area-averaged 10 m v-wind for the regions of 120–140°E, 25–40°N and 110–130°E, 10–25°N, and the leading PCs of our EA winter climate modes. The results are 0.311 and −0.293 for the first and second PC, respectively (both significant to the 99% level). Thus the EA winter climate modes are closely related to the EA winter monsoon variations.

In summary, we have studied the circulation patterns associated with the two dominant modes of EA winter climate variability. Based on observations, the first and second modes are strongly correlated with fluctuations of SCA and EU patterns, respectively. Comparison with

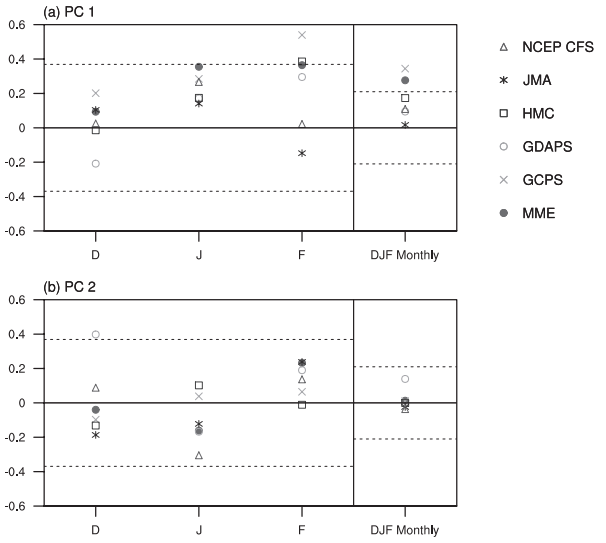

Fig. 7. Correlation coefficients between projection coefficients for model simulations and observed PC time series for the (a) first mode and (b) second mode for each month, and those based on monthly values within the whole December-February period. See text for details. Dashed lines denote the threshold values for the 90% significance level.

GCM hindcast results shows that models are able to simulate well the leading patterns of the EA winter climate variability. In the next section, we will examine the predictability of these circulation modes based on the APCC MME hindcast experiments, as well as the MME EA climate prediction during ENSO.

4. East Asian winter climate predictability in multi-model ensemble

4.1 Predictability of the EA winter climate modes

In the previous section, the ability of individual models in capturing the dominant patterns of EA winter climate variability was emphasized. In this section, the predictability of EA climate is further studied, focusing on the models' skill in reproducing the fluctuations of the two leading EA climate modes in the hindcast simulations. To correctly assess the reproducibility of the temporal variations of these modes, the monthly circulation anomalies from models were projected onto the EOF patterns from observations. The resulting "projection coefficients"— i.e. time series based upon the projection of hindcast simulations onto the observed EA climate mode patterns- are then compared with the observed PC time series. Figure 7 shows the temporal cor-

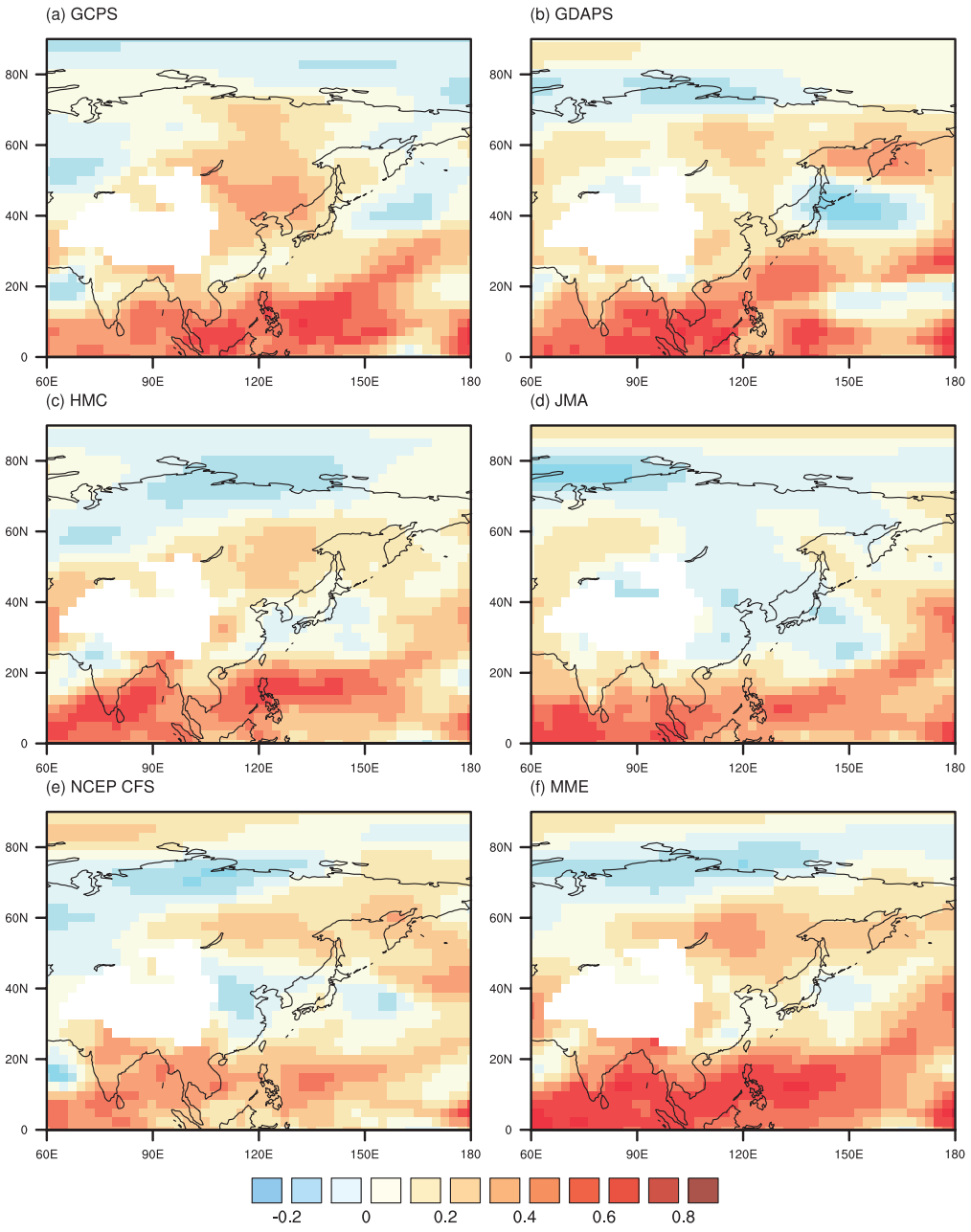

Fig. 8. Temporal correlation coefficients between the observed and the model monthly mean 850-hPa temperature taken from the whole DJF period for (a) GCPS, (b) GDAPS, (c) HMC, (d) JMA, (e) NCEP CFS and (f) MME average.

relation between the observed PCs and corresponding projection coefficients from individual model simulations and their MME average. Here, the MME mean is computed by taking a simple (un-weighted) average of the ensemble mean from each model experiment. It can be seen that, in general, the correlation is rather low. Based on the data comprising all months within DJF, there is evidence that the first EA winter climate mode is more predictable than the second mode. More specifically, both the MME and GCPS predictions are well cor-

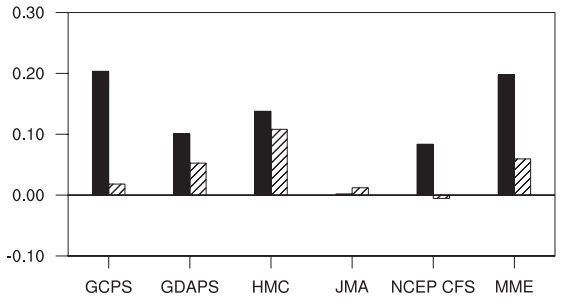

Fig. 9. Temporal correlation coefficients between the observed and the model monthly mean 850-hPa temperature, averaged over the region of 75–135°E, 40–60°N, based on the original data (solid bars) and data with signals associated with the leading EA winter climate mode removed (hatched bars). Correlations are computed based on data from all months within the DJF season.

related with the observed PC time series for the leading mode (significant above the 90% level). On the other hand, none of the model prediction for the second mode is significantly correlated with observations. In terms of monthly comparison, it can be seen that the MME captures the variations of the first EA climate mode in January and February (two individual models can also predict such its variation in February). For the second mode, however, almost none of the models accurately predict its temporal variation. The only exception to that is the output from GDAPS in the December period.

We have also computed the temporal correlation between the observed and model predicted monthly mean 850 hPa temperature. Figure 8 shows the results from each model as well the MME mean based on all months with the DJF period. In general, model predictions have skill over the tropical southeast to east Asian region (south of 20°N), especially over the oceans. However, over the Asian landmass there is a marked variation of skills among temperature predictions given by different hindcast datasets. For the MME mean, it is noteworthy that moderate prediction ability is found in the mid-to-high latitudes over continental East Asia (starting from 90°E including Lake Baikal up to the Asian coast). GCPS result shows even higher correlation in the same region. In contrast, the JMA monthly temperature predictions give a negative correlation. Comparison with the results from Fig. 7a suggests that the performance of each model in this domain could be associated with its skill in capturing the temporal variation of the first EA winter climate mode. This is consistent with the fact that the aforementioned region largely coincides with the center of action for the temperature field of this leading mode.

To ascertain the role of the first EA climate mode on the prediction ability over the aforementioned region, we have constructed new time series for the 850 hPa temperature by removing signals associated with this mode. This is achieved by subtracting a time series defined as the product of the leading PC (or model projection coefficients) and the associated temperature pattern from the original data. Temporal correlation coefficients between observations and model results are then recalculated based on this new set of temperature values. Figure 9 shows the results, together with the original correlation coefficient, averaged over the region of 75–135°E, 40–60°N. It can be seen that there is a marked reduction of skill for GCPS, NCEP CFS, MME average, and, to a lesser extent, HMC and GDAPS runs when the temperature fluctuations associated with the first EA winter climate mode are taken out. On the other hand, the JMA prediction skill in this area is not affected. This confirms our hypothesis that the first mode plays a crucial role on the climate predictability over the northeastern part of Asia. In particular, since JMA has relatively poor performance in predicting its time variation, the removal of information concerning this mode has no effect on its prediction. On the other hand, removing climate signals of the first EA climate mode will strongly affect other models that show some skill in capturing its variability.

Overall, it is found that the ability in predicting the leading EA winter climate mode varies substantially from one model to another. Such difference in skills has a strong impact on models' ability in predicting the temperature variations over the mid-to-high latitude EA land region. There is also evidence that the first mode is more predictable compared with the second mode. In fact, the second mode appears to have little predictability based on hindcast data from both individual models and the MME mean.

4.2 Wintertime circulation changes during ENSO

To assess the impact of ENSO on the EA winter climate, the 850 hPa temperature and winds are regressed onto the Nino3 index in DJF based on observations. Results are shown in Fig. 10. During early boreal winter, significant warming can be found over Indochina to the southern tip of the Indian subcontinent, which is accompanied by anomalous southwesterly over South Asia. Over the Philippines, anti-cyclonic flow in the low levels can be clearly seen. The broad-scale low-level anticyclone over South to Southeast Asia is con-

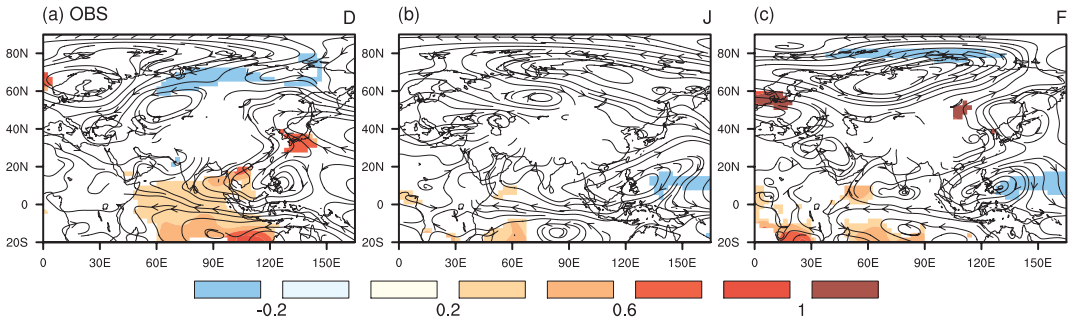

Fig. 10. Regression maps of the monthly mean 850-hPa temperature (shading, see scale at bottom; units: °C) and winds (streamlines) from observations onto the Nino3 index for (a) December, (b) January and (c) February. Temperature anomalies exceeding the 95% significance level are denoted by shading.

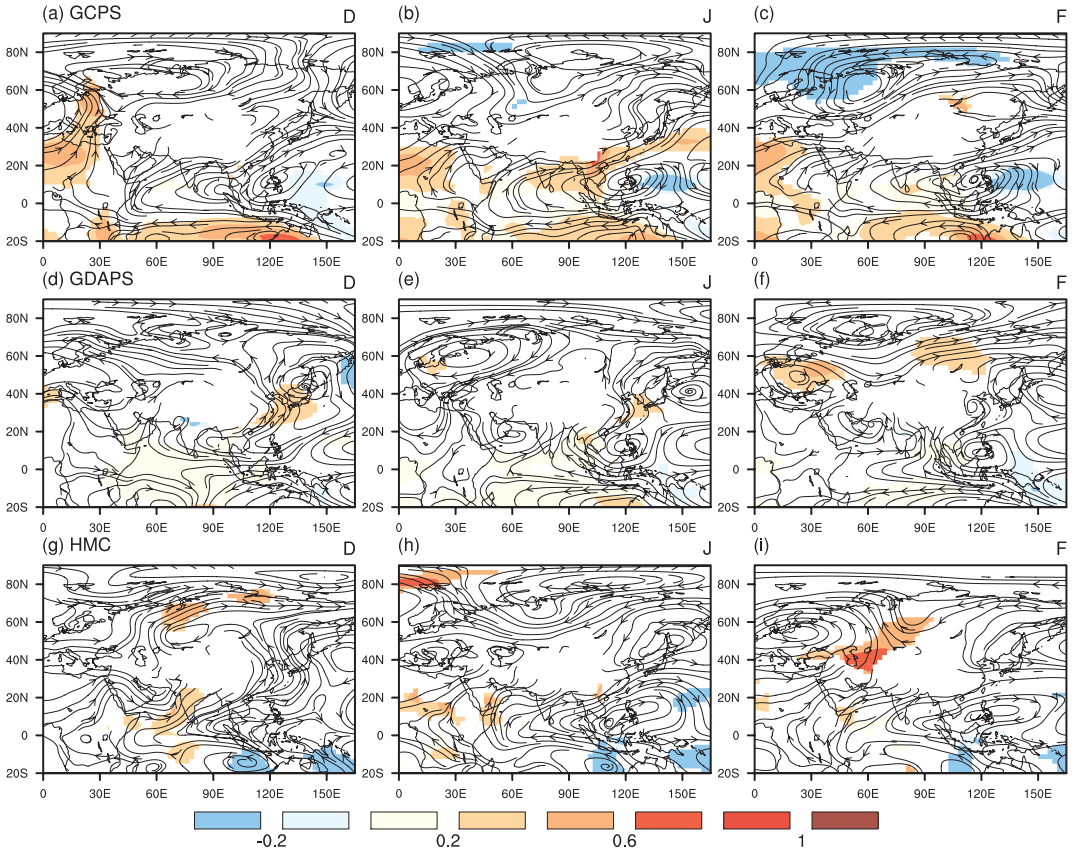

Fig. 11. Same Fig. 10 but for (a, b, c) GCPS, (d, e, f) GDAPS and (g, h, i) HMC.

sistent with the Rossby wave response to the suppressed convection over the equatorial western Pacific typically found during the warm ENSO phase (see, e.g., Lau and Wang 2005). As time progresses, the eastward development and migration of the Philippines Sea anticyclone can also be discerned (Wang et al. 2000). Overthe subtropical to midlatitude East Asia, significant warm temperature anomalies can be found covering the southern to central part of Japan as well as the Korean peninsula in December. Such mid-latitude warming signals

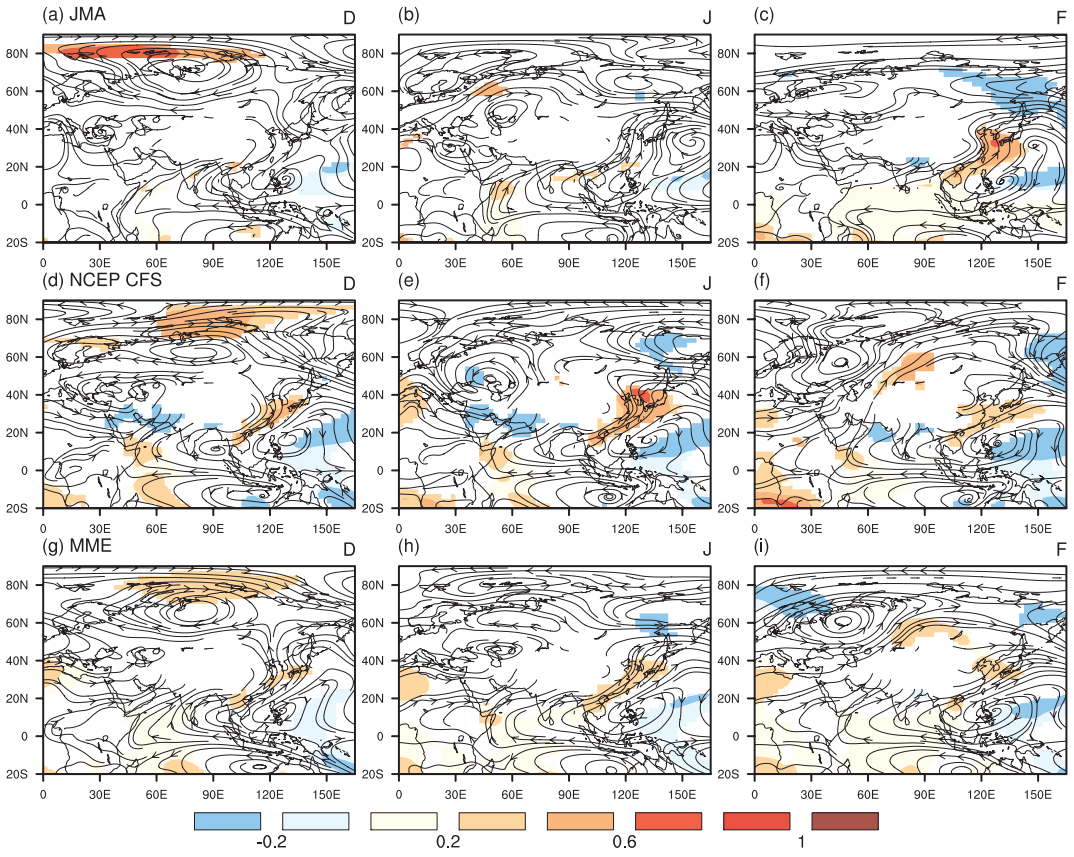

Fig. 12. Same Fig. 10 but for (a, b, c) JMA, (d, e, f) NCEP CFS and, (g, h, i) MME average.

are due to warm temperature advection by the southeasterly wind branch associated with a prominent anticyclone anchored over the north Pacific around 25–60°N. Also, a large-scale tri-pole pattern in temperature over the Eurasian continent can be discerned during early boreal winter. This observed circulation feature bears some resemblance to the second EA winter climate mode (see Fig. 5). (Further calculation indicates that the pattern correlation between the ENSO regression and the second EA mode patterns, for the area of 10–90°N, 0–160°E, exceeds the value of 0.6.) However, warmer than normal conditions in East Asia appear to dissipate quickly in the mid winter season. In February, during the course of the ENSO cycle, the aforementioned anticyclone is still discernable but has weakened considerably. On the other hand, during the late winter season, warming signals emerge over the confined landmass near Lake Baikal and northeastern Asia. Such warming over the inland region is consistent with the anomalous low-level westerlies to southwesterlies (and also southeasterlies in further southeastern locations) which appear in the regression map during February. (Further analysis of the temperature advection supports the idea that warming is brought about by the low-level wind anomalies in the region; figures not shown). In general, the abovementioned ENSO impacts on the EA winter climate inferred from regression maps are also found in composites based on El Nino minus La Nina events (figures not shown).

The same regression analysis is performed based on individual model as well as the MME mean data. Results are shown in Figs. 11 and 12. It can be seen that all models are able to reproduce the anomalous southwesterly flow over Southeast Asia and the Philippine Sea anticyclone during the warm phase of ENSO, albeit with timing different from observations in some models. However, the hindcast prediction over the mid-to-high latitude East Asia can differ considerably from the observed, depending on the model being considered. In particular, the evolution of the low-level ridge

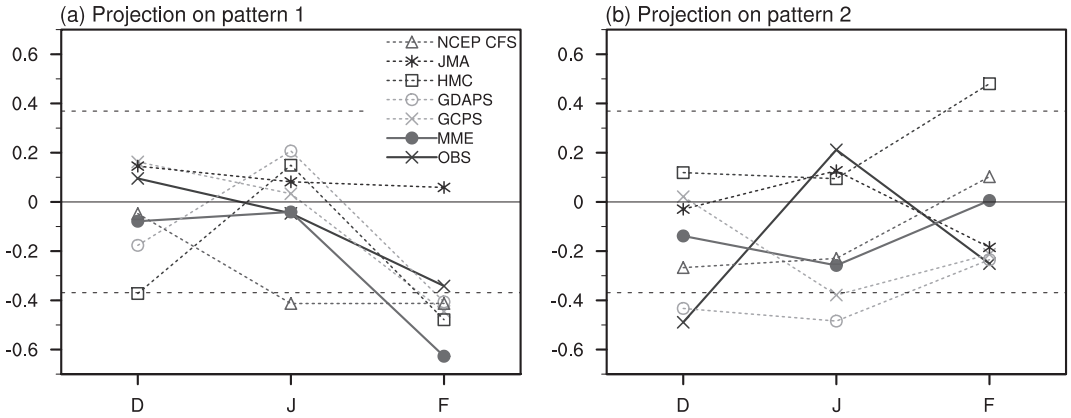

Fig. 13. Correlation between the Nino3 index and projection coefficients for model simulations (dashed lines) and their MME average (solid line with circle marker), as well as the same correlation based on the observed PC time series (solid line with cross marker) for (a) the first mode and (b) second mode for each month within the DJF period. Dashed lines denote the threshold values for the 90% significance level.

over western North Pacific near Japan is not correctly captured in most models. For the GCPS runs, this low-level ridge is almost missing (see Fig. 11). For NCEP CFS and JMA hindcasts, the simulated anticyclone becomes mature in January and February, respectively (see Fig. 12). This is in contrast to observations in which there is strong ridging over northern Japan during December, followed by rapidly dissipated signals in the following months (see Fig. 10). Finally, the MME prediction also gives a relatively weak low-level ridge over the western North Pacific and moderate warming in midlatitude costal East Asia during warm ENSO events. Such warming associated with the ridge, however, also tends to be more sustained throughout the winter season in the model environment, again in contrast to the observed ENSO impact on the EA winter climate. This is probably related to the late onset of this anticyclone in some of the models in the MME.

As shown before, ENSO affects the climate over more in-land regions during late boreal winter based on observations (see Fig. 10c). Inspection of the MME hindcast runs shows that similar circulation changes, namely warming near Lake Baikal and in the northeastern part of Asia during February, can be discerned in all models except JMA (see Figs. 11 and 12). This result concerning the JMA historical prediction is consistent with its low skill in temperature prediction over the northeastern Asian landmass (Fig. 8). GDAPS and GCPS runs show anomalous southwesterlies over northern Eurasia and warming signals in the vicinity of Lake Baikal, very similar to those based on observations. HMC and NCEP CFS runs also show warm anomalies in continental East Asia that are, however, displaced to the west. Hence, the MME mean prediction gives warmer than normal conditions around Lake Baikal and to its west, accompanied by anomalous low-level southwesterlies, in late boreal winter during the warm phase of ENSO.

The ENSO impact on the EA winter climate and the performance of the MME historical predictions are summarized in Fig. 13. It shows the correlation coefficients between the monthly values of the Nino3 index and the projection coefficients for the first and second EA climate modes based on individual models, the MME mean as well as observations (results for the latter are the same as those presented in Table 2). It can be seen that the correlation between the first PC from observations and the Nino3 index during the whole DJF period is not significant. Most models also give low correlation for this leading mode in December and January (except in February when the signals from some models and the MME mean are significantly correlated with the Nino3 index for the same month).

Observations also show that the Nino3 index is significantly correlated with the second PC in December, followed by weaker correlation in subsequent months. The strong negative correlation is in accordance with circulation changes portrayed in December during the warm ENSO phase, in which warm anomalies over southern Japan and Korea and the accompanying circulation (see Fig. 10a) will give rise to a strong and negative projection onto the second EA climate mode (see Fig. 5).

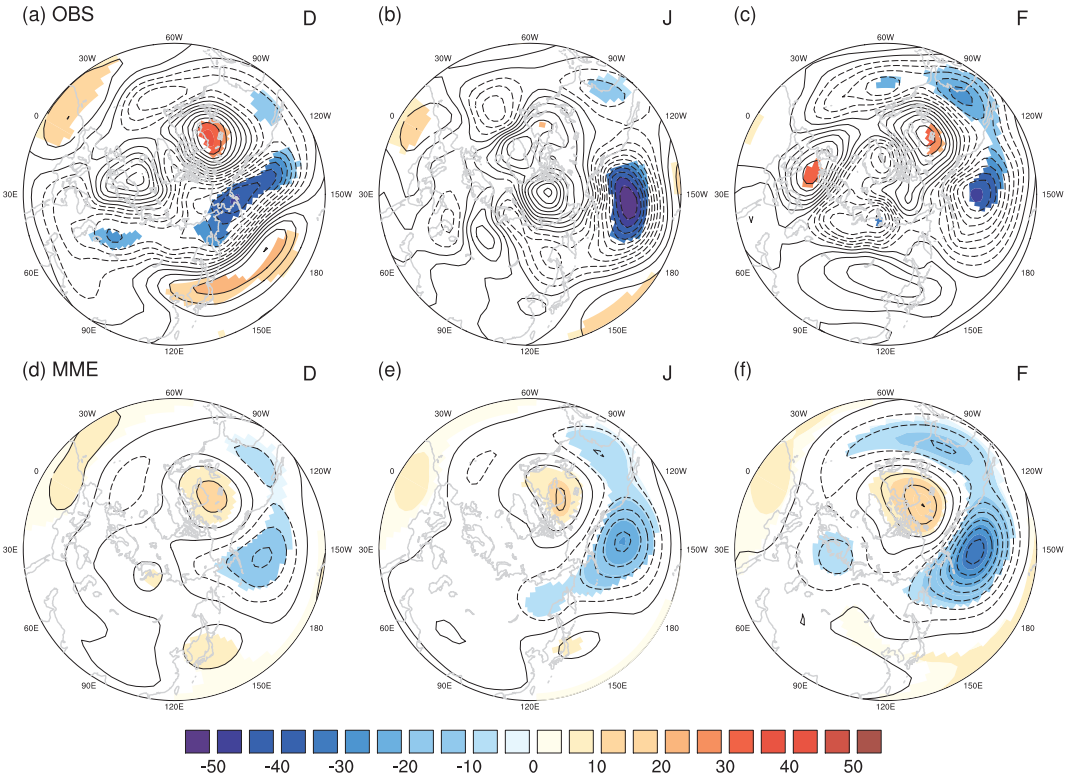

Fig. 14. Regression coefficients of the monthly 500-hPa geopotential height (contours in interval of 5 m, with negative values denoted by dashed lines) from observations and MME average onto the observed Nino3 index for (a, d) December, (b, e) January and (c, f) February. Shading denotes values exceeding the 95% significance level.

The time of occurrence of the second mode and ENSO, however, is not well reproduced by most models (except GDAPS). In fact, most models (and hence the MME mean) give a weakly negative, but otherwise steady, projection of the ENSO impact onto the second mode.

Here we also examine the circulation changes during ENSO as revealed in other meteorological variables. Figure 14 gives the regression coefficients of the monthly mean 500 hPa height field onto the Nino3 index based on observations as well as the MME mean hindcast. It can be seen that the MME hindcast gives a reasonable response over the PNA region. However, the model predicted field is strikingly weak and shows no ability over Eurasia. In particular, results from observations show a strong ridge over the North Pacific spanning costal East Asia and the dateline during early boreal winter. Connected with this is a string of strong perturbations located further west in northern Eurasia. The Eurasian wave train, and especially the ridge anchored at the western North Pacific, is seen to decrease in amplitude as time progresses. On the other hand, in the MME hindcast there is no obvious wave train in the high latitudes. Instead, there is only a weak anomalous high over Japan which persists throughout the winter season. Overall, it is obvious that the MME mean gives an impact of ENSO on the Eurasian sector that is very different from observations.

Figure 15 shows the same 500 hPa height field regression onto the Nino3 index in December for both observations and MME mean hindcast, together with the associated wave activity flux based on the formulism of Takaya and Nakamura (2001). (Note that, because of the weak model response, the MME results are plotted using a convention different from that for observations.) Observations show a wave train in the high-latitude region, which is characterized by a positive height anomaly over northern Europe, negative anomaly over north to northeastern Asian continent, and positive anomaly near Japan and further east. It is noteworthy that these centers of action over Eurasia are largely

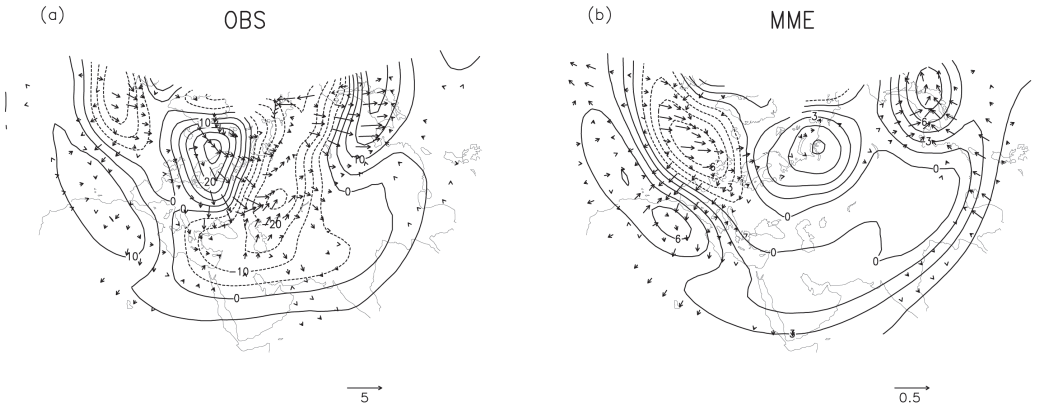

Fig. 15. Regression of 500 hPa geopotential height onto the Nino3 index for December (contours) and their accompanying wave-activity flux (arrows) based on (a) observations and (b) MME simulations. Note the different plotting conventions for observations (contour intervals: 5 m) and MME results (contour interval: 1.5 m). See arrow scales on bottom right (units: 10^{-6} ms^{-2}). Vectors are displayed only at locations where the absolute magnitude of their divergence is greater than 0.5×10^{-6} ms^{-2} (0.05×10^{-6} ms^{-2}) for observations (MME).

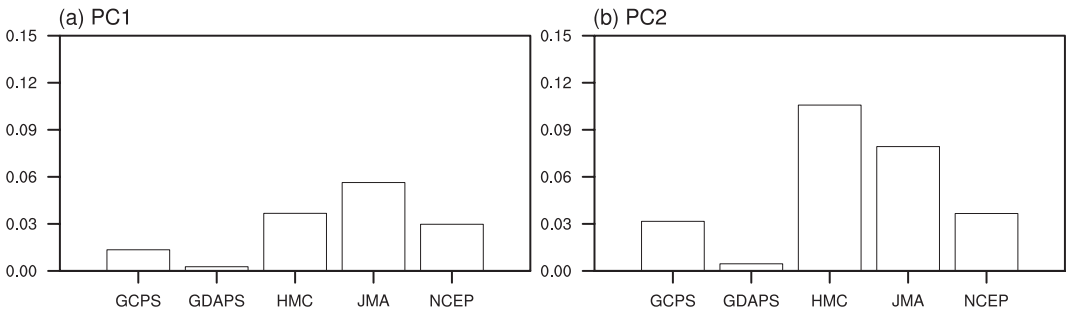

Fig. 16. Potential predictability of the model simulated PC time series for (a) the first mode and (b) the second mode based on monthly values within the whole DJF period.

collocated with those related to the second EA climate mode in the geopotential height in December (see Fig. 4d). The related wave activity indicates Rossby wave energy dispersion along the high-latitude wave train into the high pressure system over Japan/coastal East Asia. To summarize, these results suggest that circulation changes very similar to the second EA climate mode are excited during ENSO in early boreal winter, probably due to wave activity coming from more western locations in Eurasia.

The MME results, on the other hand, give a different picture. There is no obvious wave train across the northern Eurasian continent. Although forcing exists in the subtropical Atlantic, the wave activity seems to be reflected equator-ward over the far eastern Atlantic/European region instead of initiating a Eurasian wave train. Focusing on the positive height anomaly over Japan, there is relatively weak wave activity entering into this system from the west. Instead, in the model environment wave activity comes from the south in the East Asian/Pacific sector. Inspection of individual model results reveals that the wave activity in the Pacific sector exists mainly in the GDAPS and NCEP CFS simulations. Such forcing from the western Pacific side, which is not found in observations, is likely the reason why the western North Pacific high is maintained throughout the DJF period in the MME mean hindcast.

5. Discussions and summary

We have diagnosed the EA winter climate variability in five GCMs participating in the APCC MME seasonal

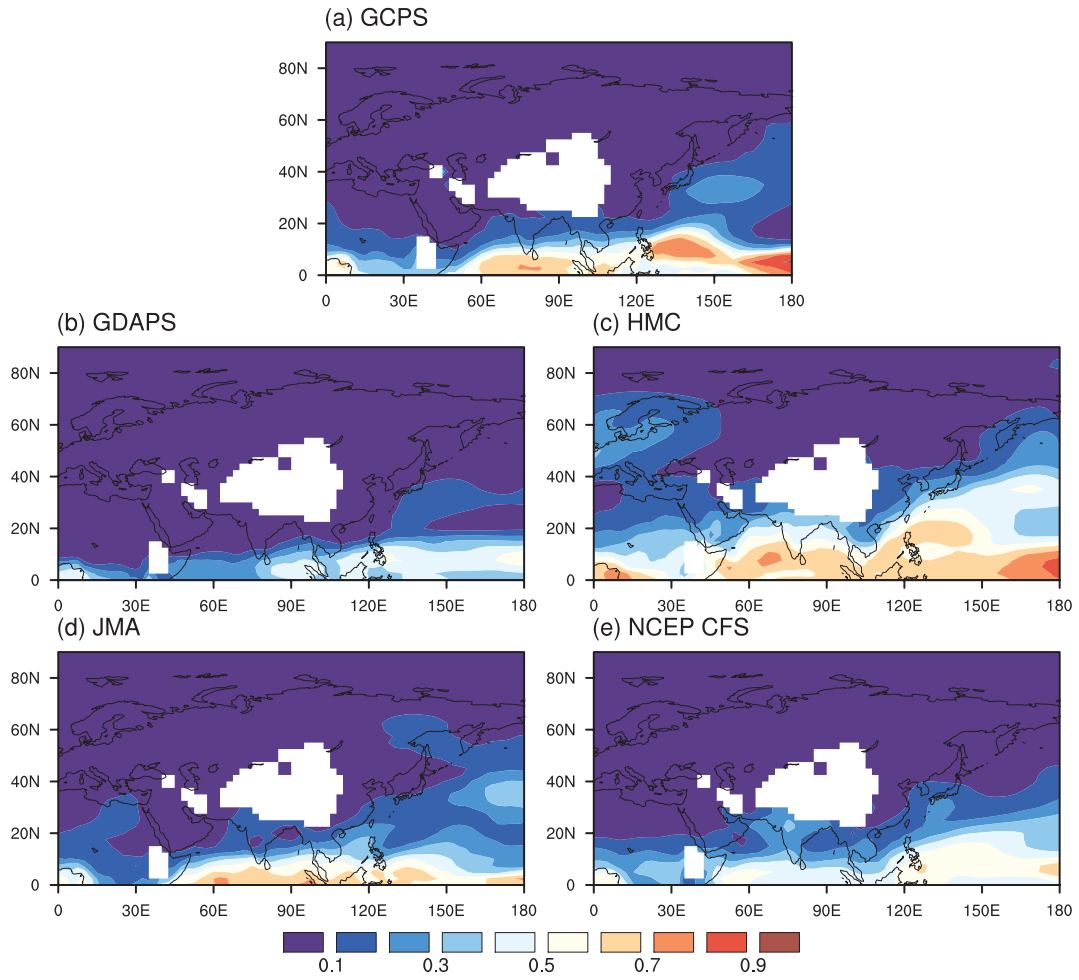

Fig. 17. Potential predictability of model monthly 850-hPa temperature within DJF for (a) GCPS, (b) GDAPS, (C) HMC, (d) JMA and (e) NCEP CFS.

prediction system. Model hindcast datasets covering the boreal winter from 1983/1984–2003/04 have been used. Based on multivariate EOF analysis of the observed monthly low-level wind and temperature, the first two leading modes of EA climate variability have been examined. The first mode is characterized by large-scale circulation features. During its positive phase, there is cooling over a broad region from the northwestern flank of the Siberian high to the northeastern part of Asia. In the positive phase of the second mode, which exhibits more regional-scale circulation changes, a negative temperature anomaly is present over coastal East Asia including the eastern part of China, Korean peninsula and Japan. It is found that the leading EA climate mode is linked to the SCA pattern, while the second mode is strongly associated with the EU pattern. Both of these EA climate modes modulate the strength of the Siberian high. In general, the EA wintertime variability is well captured in the model environments of the GCMs being examined. Further analyses of the dominant patterns of variability show that the two leading EA climate modes are also well reproduced in all model hindcasts.

The predictability of the EA winter climate modes based on the MME hindcast datasets has also been examined. In general, models have much difficulty in predicting the observed temporal variations of these modes, despite of the fact that these circulation patterns are well simulated in the model environments. There is evidence that there is some predictability for the leading mode. In particular, the observed and model simulated temporal variations of the first mode are significantly correlated for the GCPS run as well as the MME mean output. The

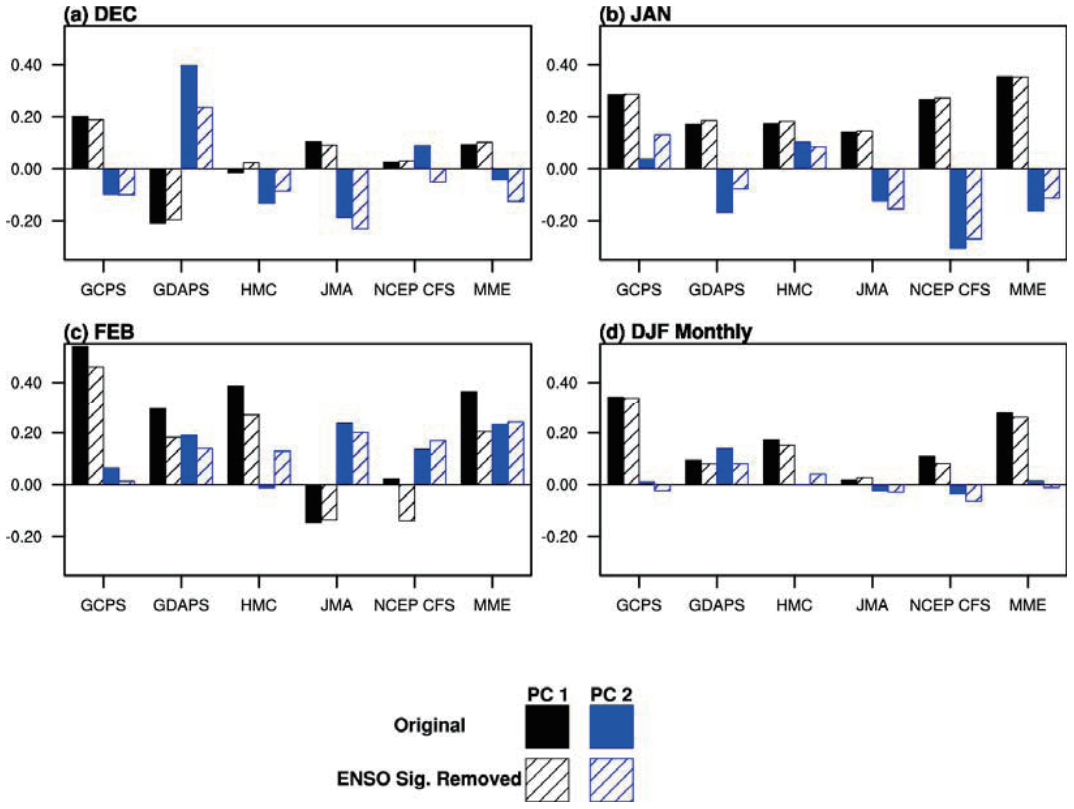

Fig. 18. Temporal correlation coefficients between the observed PC time series and model projection coefficients for the leading EA climate modes, based on original data (solid bars) and data with ENSO signals removed (hatched bars) for (a) December, (b) January, (c) February, and (d) all months within the DJF season. Black and blue bars denote, respectively, the first and second PC time series. Note that the results for the original data are the same as those presented in Fig. 7.

leading mode is found to be especially important for the winter monsoon predictability over northeast Asia. Models' ability of predicting the winter climate in the mid-to-high latitude East Asia (from Lake Baikal to the East Asian coast) is strongly related to their skill in capturing the fluctuation of this mode. On the other hand, there is almost no skill in predicting the temporal variations of the second mode.

To assess the impact of ENSO on the EA winter climate, the 850 hPa temperature and winds are regressed onto the December, January and February values of the Nino3 index. Anomalous southwesterlies over South Asia and low level anti-cyclonic flow over the Philippines are seen during the warm ENSO phase. Significant warm temperature anomalies covering the southern to central part of Japan as well as the Korean peninsula are found in December. However, they quickly dissipated in January, and weakened temperature signals remained in February. All models are able to reproduce the anomalous southwesterly flow over Southeast Asia and the Philippine Sea anticyclone during the warm phase of ENSO. However, predictions based on the MME mean (and by some models) give a moderate warming in midlatitude coastal East Asia, which tends to persist throughout the winter season. Also, most models cannot capture the timing and the strength of the observed second EA climate mode variations during ENSO. Warm signals during the late winter season of an El Nino are observed over Lake Baikal to northeastern Asian landmass. Most models also give analogous warming in the high latitudes near Lake Baikal and to its west during February. The circulation changes during ENSO in other meteorological variables are also examined. Wave activity analysis shows Rossby wave energy coming from Eurasia into the anomalous high over the western North Pacific, which is manifested as a strong

ridge affecting Japan, Korea, and eastern China, in early boreal winter during El Nino years. The Eurasian wave train, however, is either too weak or absent in the model simulations. Instead, there is only a weak anomalous high over Japan which persists throughout the winter season. Further study shows that it is sustained by forcing coming from the tropical western Pacific in the model environment.

Our results point to the salient fact that the EA winter climate is difficult to predict in the current framework of dynamical seasonal prediction. We have computed the potential predictability (Rowell 1998) of the two leading EA climate modes, as well as that for the wintertime EA temperature, based on output from each model. Results are shown in Figs. 16 and 17. It can be seen that, indeed, the predictability of the EA modes is very low, which is the case for all models (see Fig. 16). Consistently, there is also low potential predictability of the temperature in the mid latitudes (see Fig. 17). The above suggests that the internal variability of the wintertime climate in extratropical East Asia makes the latter difficult to predict in the framework of seasonal climate prediction. On the other hand, there is still discernable variation among the prediction skills of different models. We speculate that this is due to different model's inability in reproducing the actual atmospheric responses to external forcings (Kang and Shuka 2006). Whether our inability to reproduce the EA climate variation is due to model inadequacy or intrinsic predictability limits, remains an open question. More studies using large member ensemble are needed to distinguish the boundary forced response from variability owning to internal dynamics.

Finally, it is interesting that the first EA winter climate mode seems to be more predictable than the second mode. Yet, especially in December, the ENSO impact is seen to project stronger on the second mode than on the first mode (see also Table 2). To further delineate the role of ENSO on the predictability of the two EA climate modes, we have removed the ENSO signals from both observations and the model datasets, and then calculated the models' skill in predicting these modes again. Figure 18 shows the correlation between the observed PCs and model projection coefficients, before and after removing the ENSO signals. MME results based on all months within DJF indicate that ENSO has almost no impact on the predictability of these two EA climate modes (see Fig. 18d). Only in the GDAPS hindcast prediction for the second mode, does ENSO seem to exert some influence. Inspection of the correlation for each individual month suggests that this is mainly due to the drop in skill of GDAPS in December, when the ENSO component of the second PC (and the corresponding model projection coefficients) is taken out (see Fig. 18a). Overall, it is clear that the stronger predictability of the first EA winter climate mode is not related to ENSO. Whether it is due to external forcing other than ENSO or perhaps the presence of some precursory signals needs to be explored in future.

Acknowledgements

We would like to thank Jong-Seong Kug, June-Yi Lee, Bin Wang and Wen Chen for their encouragement and helpful suggestions during various stages of this study. The authors also appreciate those institutes participating in the APCC multi-model ensemble operational system for providing the hindcast experiment data.

References

Barnston, A. G., and R. E. Livezey, 1987: Classification, seasonality and persistence of low-frequency atmospheric circulation patterns, *Mon. Wea. Rev.*, **115**, 1083–1126.

Bengtsson, L, U. Schlese, E. Roechner, M. Latif, T. P. Barnett, and N. Graham, 1993: A two-tiered approach to long-range climate forecast, *Science*, **261**, 1026–1029.

Bueh, C., and H. Nakamura, 2007: Scandinavian pattern and its climatic impact, *Quart. J. Roy. Meteor. Soc.*, **133**, 2117–2131.

Chan, J. C. L., 2005: The Asian winter – Australian summer monsoon: A review of the East Asia winter monsoon, in *The Global Monsoon System: Research and Forecast*, edited by C.-P. Chang, B. Wang, and N.-C. G. Lau, WMO/TD No. 1266.

Chen, W., H.-F. Graf, and R.-H. Huang, 2000: The interannual variability of East Asian winter monsoon and its relation to the summer monsoon, *Adv. Atmos. Sci.*, **17**, 48–60.

Covey, C, K. M. AchutaRao, U. Cubasch U, and Coauthors, 2003: An overview of results from the Coupled Model Intercomparison Project (CMIP), *Glob. Planet. Change*, **37**, 103–133.

Gong, D.-Y., S.-W. Wang, and J.-H. Zhu, 2001: East Asian winter monsoon and Arctic oscillation, *Geophys. Res. Lett.,* **28**, 2073–2076.

Jhun, J.-G., and E.-J. Lee, 2004: A new East Asian winter monsoon index and associated characteristics of the winter monsoon, *J. Climate*, **17**, 711–726.

Kalnay, E, M. Kanamitsu, R. Kistler, and Coauthors, 1996: The NCEP/NCAR 40-year reanalysis project, *Bull. Amer. Meteor. Soc.*, **77**, 437–471.

Kanamitsu, M., K. Tada, T. Kudu, and Coauthors, 1983: Description of the JMA operational spectral model, *J. Meteor. Soc. Japan*, **61**, 812–827.

Kang, I.-S., J.-Y. Lee, and C.-K. Park, 2004: Potential predictability of summer mean precipitation in a dynamical seasonal prediction system with systematic error correction, *J. Climate*, **17**, 834–844.

Kang, I.-S., and J. Shukla, 2006: Dynamic seasonal prediction and predictability of the monsoon, in *The Asian Monsoon*, edited by B. Wang, Praxis Publishing Ltd.

Kug, J.-S., J.-Y. Lee, and I.-S. Kang, 2007: Global sea surface temperature prediction using a multi-model ensemble, *Mon. Wea. Rev.*, **135**, 3239–3247.

Lau, K. M., and M. T. Li, 1984: The monsoon of East Asia and its global association-A survey, *Bull. Amer. Meteor. Soc.*, **65**, 114–125.

Lau, N.-C., and B. Wang, 2005: Monsoon-ENSO interactions, in *The Global Monsoon System: Research and Forecast*, edited by C.-P. Chang, B. Wang, and N.-C. G. Lau, WMO/TD No. 1266.

Murakami, T., 1979: Winter monsoonal surge over East and Southeast Asia, *J. Meteor. Soc. Japan*, **57**, 133–158.

Moorthi, S., H.-L. Pan, and P. Caplan, 2001: Changes to the 2001 NCEP operational MRF/AVN global analysis/forecast system. *NWS Tech. Procedures Bulletin 484*, 14 pp. [Available online at http://www.nws.noaa.gov/om/tpb/484.htm.]

Pacanowski, R. C., and S. M. Griffies, cited 1998: MOM 3.0 manual, NOAA/GFDL. [Available online at http://www.gfdl.noaa.gov/~smg/MOM/web/guide_parent/guide_parent.html.]

Pan, H. L., and F. X. Zhou, 1985: The 10–20 day tropical-midlatitude interaction during winter monsoon season, *J. Meteor. Soc. Japan*, **63**, 829–843.

Park, H., B. K. Park, D. K. Rha, and J. Y. Cho, 2002: An improvement of global model in 2001, *KMA/NWPD Tech. Rep.*, 2002-1 (In Korean).

Roads, J. O., S.-C. Chen, and F. Fujioka, 2001: ECPC's Weekly to Seasonal Global Forecasts, *Bull. Amer. Meteor. Soc.*, **82**, 639–658.

Rowell, D. P., 1998: Assessing potential seasonal predictability with an ensemble of multidecadal GCM simulations, *J. Climate*, **11**, 109–120.

Saha, S, S. Nadiga, C. Thiaw, and Coauthors, 2006: The NCEP Climate Forecast System, *J. Climate*, **19**, 3483–3517.

Takaya, K., and H. Nakamura, 2001: A formulation of a phase-independent wave-activity flux for stationary and migratory quasigeostrophic eddies on zonally varying basic flow, *J. Atmos. Sci.*, **58**, 608–627.

Takaya, K., and H. Nakamura, 2005: Mechanisms of intraseasonal amplification of the cold Siberian high, *J. Atmos. Sci.*, **62**, 4423–4440.

Thompson, D. W. J., and J. M. Wallace, 2000: Annular modes in the extratropical circulation. Part I: Month-to-month variability, *J. Climate*, **13**, 1000–1016.

Tolstykh, M. A., 2003: Variable resolution global semi-Lagrangian atmospheric model. Russ, *J. Numer. Anal. Math. Modelling*, **18**, 347–361.

Wallace, J. M., and D. S. Gutzler, 1981: Teleconnections in the geopotential height field during the northern hemisphere winter, *Mon. Wea. Rev.*, **109**, 784–812.

Wang, B., 1992: The vertical structure and development of the ENSO anomaly mode during 1979–1989, *J. Atmos. Sci.*, **49**, 698–712.

Wang, B., R. Wu, and X. Fu, 2000: Pacific-East Asian teleconnection: How does ENSO affect East Asian climate?, *J. Climate*, **13**, 1517–1536.

Wang, L., W. Chen, and R. Huang, 2008: Interdecadal modulation of PDO on the impact of ENSO on the east Asian winter monsoon, *Geophys. Res. Lett.*, doi: 10.1029/2008GL035287.

Wu, B., and J. Wang, 2002: Winter Arctic oscillation, Siberian high and East Asian winter, *Geophys. Res. Lett.*, doi:10.1029/2002GL015357.

Zhang, Y., K. R. Sperber, and J. S, Boyle, 1997a: Climatology and interannual variation of East Asian winter monsoon: Results from the 1979–1995 NCEP/NCAR reanalysis, *Mon. Wea. Rev.*, **125**, 2605–2619.

Zhang, Y., K. R. Sperber, J. S. Boyle, and Coauthors, 1997b: East Asian winter monsoon: results from eight AMIP models, *Climate Dyn.*, **13**, 797–820.

Zhu, C., W.-S. Lee, H. Kang, and Coauthors, 2005: A proper monsoon index for seasonal and interannual variations of the East Asian monsoon, *Geophys. Res. Lett.*, doi:10.1029/2004GL021295.

Zwiers, F. W., and H. von Storch, 1995: Taking serial correlation into account in test of the mean, *J. Climate*, **8**, 336–351.